Neodymium electrowinning into copper-neodymium alloys by mixed oxide reduction in molten fluoride media

Mihaela Raluca Ciumag, Mathieu Gibilaro, Laurent Massot, Richard Laucournet, Pierre Chamelot

Neodymium electrowinning into copper-neodymium alloys by mixed oxide reduction in molten fluoride media

M. Ciumag[a,b], M. Gibilaro[a,*], L. Massot[a], R. Laucournet[c], P. Chamelot[a]

[a] *Laboratoire de Génie Chimique UMR CNRS 5503, Université Paul Sabatier, 118 route de Narbonne, 31069 Toulouse Cedex 9, France*
[b] *CEA-Tech Midi-Pyrénées, 135 avenue de Rangueil, 31400 Toulouse, France*
[c] *CEA Grenoble LITEN, 17 rue des Martyrs, 38054 Grenoble Cedex 9, France*

A B S T R A C T

The possibility of neodymium electrowinning from neodymium oxide using a reducing agent (RA) produced in-situ by solvent reduction was investigated in molten LiF–CaF_2–Li_2O between 900 °C and 1040 °C. Nd_2O_3 galvanostatic electrolyses were performed and reaction products were analyzed by SEM, XRD and electron-probe microscopy. Metallic neodymium was not directly obtained, due to several limitations for Nd_2O_3 reduction: low electrical conductivity, unfavourable Pilling–Bedworth coefficient and formation of a dense insulating CaO layer on the sample surface.

Consequently, the reduction of a pellet made of a neodymium oxide-metallic oxide mixture was carried out as an alternative pathway. Nd_2O_3-CuO reduction led to metallic neodymium production in the form of liquid Cu-Nd alloys. A reaction mechanism was proposed based on these experimental results:

1. Introduction

Needs of metallic neodymium and its alloys are lately increasing, particularly in the fields of magnetism, energy and high technology, as in permanent magnets, lamp phosphors and rechargeable NiMH batteries [1]. Neodymium is industrially produced by both calciothermic reduction of NdF_3, requiring several purification steps, and by molten salt electrolysis, which enables continuous operation and is more suitable for mass metal production.

Metallic neodymium electrodeposition can take place in fused chloride salts [2–13], but this process has several drawbacks, such as the evolution of chlorine gas at the anode and low faradic yield. Thus, neodymium metal is currently produced by electrowinning from neodymium oxide in a molten fluoride media containing high amounts of NdF_3 (up to 87 mass %) [14].

Several authors suggested different reduction mechanisms of Nd_2O_3 in NdF_3-based molten salt [16–19], but no agreement has been found yet. Stefanidaki et al. [15,16] detailed neodymium production in LiF–Nd_2O_3 and LiF–NdF_3–Nd_2O_3 systems. In LiF–Nd_2O_3 no characteristic signal for neodymium oxide reduction into metal was observed and metallic neodymium deposition did not occur in this molten mixture. In LiF–NdF_3–Nd_2O_3, fluoride and oxyfluoride complexes such as $[NdF_6]^{3-}$ and $[NdOF_5]^{4-}$ were proposed to be formed, and metallic neodymium was observed. The following electron transfer mechanism was suggested:

Cathode: $[NdF_6]^{3-} + 3e^- \rightarrow Nd(s) + 6F^-$

Anode: $3[NdOF_5]^{4-} \rightarrow 3/2O_2(g) + 3Nd^{3+} + 15F^- + 6e^-$

The authors concluded that electrowinning of metallic neodymium can be performed by controlled cell–voltage electrolysis in LiF–NdF_3–Nd_2O_3.

Thudum et al. [17] proposed a different reduction pathway for Nd_2O_3 in LiF-CaF_2-NdF_3, suggesting both $[NdFO_5]^{4-}$ and $[NdF_6]^{3-}$ complexes were reduced to metallic neodymium, depending on the OF/F molar ratio: for low ratios, $[NdF_6]^{3-}$ was reduced, whereas above a critical value, $[NdFO_5]^{4-}$ was reduced.

Dysinger and Murphy [18] tested Nd_2O_3 reduction in LiF–CaF_2–NdF_3 on tungsten cathode, for temperatures from 1030 °C to

1060 °C, and highlighted several side reactions occurring at the anode:

1. Nd(0) reoxidation: $Nd(0) + 3F^- \rightarrow NdF_3 + 3e^-$
2. Nd(0) reactions with the anodic gas (CO_2): $2Nd + 3CO_2 + NdF_3 \rightarrow 3NdOF + 3CO$

$3CO_2 + 2Nd \rightarrow Nd_2O_3 + 3CO$

The authors concluded metallic neodymium electrowinning from $LiF–CaF_2–NdF_3–Nd_2O_3$ was only possible at high current density (1 A cm^{-2}) and high temperature (T > 1021 °C = Nd fusion temperature).

Fe–Nd alloys were obtained by Morrice et al. [19], by Nd_2O_3 electrolysis on reactive iron cathode at 990 °C in $LiF–NdF_3$ (89 mass %). Later, Nd_2O_3 electrolysis in fused fluorides for Fe–Nd fabrication was patented by Pechiney [20]. Alloys were obtained by long duration (> 25 h) Nd_2O_3 electrolyzes on reactive iron cathode, performed in $LiF–NdF_3–BaF_2–B_2O_3$, between 750° and 1000 °C, and at constant cell voltage.

Nowadays, neodymium is industrially produced by Nd_2O_3 reduction in NdF_3-based mixtures (NdF_3 > 70 mass % [21]) using Mo, W or Fe as cathodic materials [22]. Nevertheless, several drawbacks can be pointed out for this process:

- The solubility of Nd_2O_3 is only 5 mass % (at 1100 °C) [23], which makes the oxide feeding into the electrolyte difficult to control and can lead to formation of sludge at the cell bottom [24].
- The overall cost of the industrial process is high due to the price of NdF_3 (∼ 1000 euros/kg).

The aim of this work is to investigate a lower cost production process for neodymium electrowinning from Nd_2O_3 in molten fluoride media, in absence of NdF_3 ($LiF–CaF_2$ eutectics containing Li_2O 2 mass %), by a new approach: the neodymium oxide is used as solid pellets at the cathode, similarly to the FFC—Cambridge [25] and OS processes [26], and no more as the feed material (current industrial process). The two main advantages of this approach are: firstly, Nd_2O_3 solubility limitation, encountered for the conventional electrolytic system, is eliminated. Secondly, the overall price of the process is reduced, due to the lower cost of $LiF–CaF_2–Li_2O$: 1 kg of $LiF–CaF_2–Li_2O$ mixture costs 200 euros (∼ 60 mass % LiF at 100 euros/kg, ∼40 mass % CaF_2 at 60 euros/kg and 2 mass % Li_2O at 4800 euros/kg); while 1 kg of $LiF–NdF_3$ mixture costs ∼750 euros (∼30 mass % LiF at 100 euros/kg, and 70 mass % NdF_3, at 1000 euros/kg).

With this new approach, Nd_2O_3 electroreduction was studied by linear voltammetry and galvanostatic electrolyses at different operating parameters: temperatures from 900 °C to 1040 °C and imposed currents from 0.15 to 0.8 A. Elemental analyses of compositions and microstructures (SEM, XRD and electron-probe microanalyser) were performed, and the limiting factors for Nd_2O_3 reduction into Nd in molten fluorides, in absence of NdF_3, were elucidated for the first time.

Nd_2O_3 electroreduction in presence of an electrical conducting metallic oxide was also investigated. Indeed, this strategy was already shown to be suitable for preparing Nd–Co alloys by electrochemical reduction of $Nd_2O_3–Co_3O_4$ mixtures in molten chloride media [27]. Other rare earths alloys with heavy metals, such as La–Ni [28], Ce–Co [29], Ce–Ni [30], Tb–Fe [31] and Tb–Ni [32], were also obtained by electrochemical reduction of rare earth oxides and metallic oxides mixtures.

In this study, the electrochemical behaviour of $Nd_2O_3–CuO$ was investigated at different temperatures by linear voltammetry and constant current electrolyses. Analysis of microstructures showed formation of Cu–Nd alloys and allowed proposing a reduction pathway. For high purity metallic Nd recovery, a further separation of Cu and Nd can be easily realised with electrorefining, by exploiting the electrochemical potentials of the two constituents.

2. Results and discussion

2.1. Preliminary discussion and solvent selection

Rare earth oxides can be electrochemically reduced by two different pathways, depending on their electrical conductivity:

1. Highly conductive oxides are subject to direct electrochemical reduction by FFC—Cambridge process [25], where the oxide is reduced into metal on the cathode surface.
2. Oxides presenting low electrical conductivity are subject to indirect reduction by OS process [26]. In this case, a reducing agent (produced by solvent reduction) reacts with the rare earth oxide to form a metallic phase.

Nd_2O_3 has a very low electrical conductivity ($\sigma_{650°,0,2barO2}$ = $1{,}45 \times 10^{-6}\,\Omega^{-1}\,cm^{-1}$ [33]) therefore it is expected to be reduced following the indirect OS process, as illustrated in the equation:

$$Nd_2O_3 + 3x\ RA \rightarrow 2\ Nd + 3\ RA_xO \quad (1)$$

where RA is the reducing agent and RA_xO is the oxidized form of the reducing agent.

The reducing agent (RA) could be an alkaline (K, Na, Li) or alkaline-earth metal (Ca) obtained by cathodic reduction of fluoride solvents (KF, NaF, LiF, CaF_2). The Gibbs energy of the reaction ($\Delta_rG°$) between neodymium oxide and the reducing agent indicates whether the neodymium oxide is reduced into metallic neodymium or not: if $\Delta_rG°$ is negative, the reduction of neodymium oxide by the alkaline or alkaline-earth is thermodynamically achievable. As presented in Table 1, neodymium oxide can be reduced into metallic neodymium by Ca only.

Nevertheless, because of CaF_2 too high fusion temperature (1 418 °C), a lower working temperature was chosen: $LiF–CaF_2$ eutectics (T_{fusion} = 767 °C). Because the reduction potentials of Li^+ and Ca^{2+} are close (E Li^+/Li = −5.31 V vs F_2/F^- and E Ca^{2+}/Ca = −5.33 V vs F^2/F^-), their simultaneous reduction at the cathode surface was already observed [34].

Table 1
Standard free energy data for Nd_2O_3 reduction with different alkali and alkaline-earth metals, following equation (1) at 900 °C.

RA	K	Na	Li	Ca
$\Delta_rG°$ at 900 °C (kJ mol^{-1})	863.3	713.7	154.1	−57.2

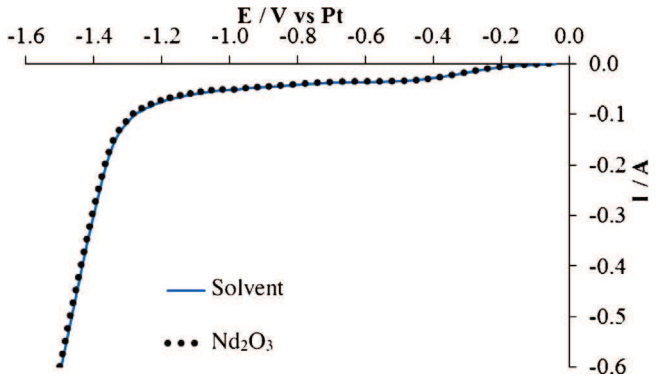

Fig. 1. Linear sweep voltammograms on Mo grid in LiF–CaF_2–Li_2O (2 mass % Li_2O) at 10 mV s^{-1} and 900 °C. Continuous line: solvent, dotted line: Nd_2O_3 pellet.

2.2. Electrochemical characterization in LiF–CaF_2 by linear sweep voltammetry

To provide O^{2-} ions in the molten fluoride media and ensure the anodic reaction, Li_2O was used. Gibilaro et al. [35] showed in LiF–CaF_2–Li_2O mixture, Li_2O had to be maintained at a concentration higher than 1 mass % to prevent the Au anode oxidation and to ensure the oxidation of O^{2-} into gaseous O_2 [36].

In this work, Nd_2O_3 reduction mechanism was studied in LiF–CaF_2–Li_2O (2 mass %). The linear voltammogram obtained at 10 mV. s^{-1} and 900 °C, is presented in Fig. 1, compared with the solvent.

The two curves display no significant difference, meaning that no specific Nd_2O_3 electrochemical reaction occurs. Therefore, its reduction is indirect and the proposed reaction pathway is the following:

$$\text{Cathode: } Ca^{2+} + 2e^- \rightarrow Ca \quad (2)$$

$$\text{Spontaneous redox reaction: } Nd_2O_3 + 3Ca \rightarrow 2Nd + 3CaO \quad (3)$$

$$\text{Anode: } 2O^{2-} \rightarrow O_2 + 4e^- \quad (4)$$

The Ca reducing agent [34] produced on the Mo cathode reduces the neodymium oxide into metallic neodymium, and the resulted O^{2-} ions are oxidized into gaseous O_2 on the gold anode.

2.3. Galvanostatic electrolyses of neodymium oxide

2.3.1. Neodymium oxide reduction

To investigate Nd_2O_3 reduction, experiments were carried out in constant current mode. Because stable reference electrodes in fluoride salts are not available yet (no accurate control of cathodic potential), the constant potential mode was not used during electrolyzes.

Several reduction tests were performed in LiF–CaF_2–Li_2O (2 mass %) at 900 °C. The theoretical charge Q_{th} needed for the reduction of one neodymium oxide pellet is calculated as follows:

$$Q_{th} = \frac{m Nd_2O_3}{M Nd_2O_3} nF \quad (5)$$

where Q_{th} is the theoretical charge calculated (C), m Nd_2O_3 is the oxide pellet weight (g), M Nd_2O_3 is the oxide molecular weight (336.48 g.mol^{-1}), n is the number of electrons exchanged per mole of Nd_2O_3, F is the Faraday constant (96,480 C mol^{-1}).

The pellet cross-section after electrolysis at $I = -0.4$ A and $t = 1320$ s (500% Q_{th}), observed by SEM, shows three different zones (Fig. 2). Quantitative electron-probe microanalysis allowed identifying the composition of these zones, as follows:

- The internal zone (1) is mainly NdOF, formed by spontaneous decomplexation of Nd_2O_3:

$$Nd_2O_3 + 2F^- \rightarrow 2NdOF + O^{2-} \quad (6)$$

This phenomenon was also observed by Nourry [37] when adding O^{2-} ions in LiF–CaF_2–NdF_3.

- Zone 2 is formed by recrystallized fluoride salts (LiF and CaF_2).
- A dense layer mainly composed of low electrical conducting CaO, formed by O^{2-} and Ca^{2+} co-precipitation, is observed overall the surface of the neodymium oxide pellet (zone 3). The CaO layer acts as a barrier, limiting the diffusion of O^{2-} from the pellet towards the molten salt, preventing the Nd_2O_3 reduction to take place. This phenomenon explains the absence of metallic Nd at the end of electrolysis.

2.3.2. Temperature influence

To increase CaO solubility in LiF-CaF_2 (from 0.5 mol % at 730 °C to 2.9 mol % at 1 000 °C, [38]) and to attempt to remove the layer on the sample surface, experiments were performed at higher temperature, where liquid metallic neodymium could be formed. Fig. 3 illustrates the cross-section of Nd_2O_3 sample after electrolysis at 1040 °C and −0.4 A (500% Q_{th}).

As expected, no CaO layer was formed on the sample surface, but X-ray diffractommetry (Fig. 4) did not highlight either the presence of metallic Nd.

When comparing Fig. 2 (900 °C) and Fig. 3 (1040 °C), it can be pointed out that the pellet structure and composition changed: Nd_2O_3 chemical decomplexation at 900 °C led to NdOF, while at 1 040 °C Nd_2O_3 clusters appeared, enhancing significantly the

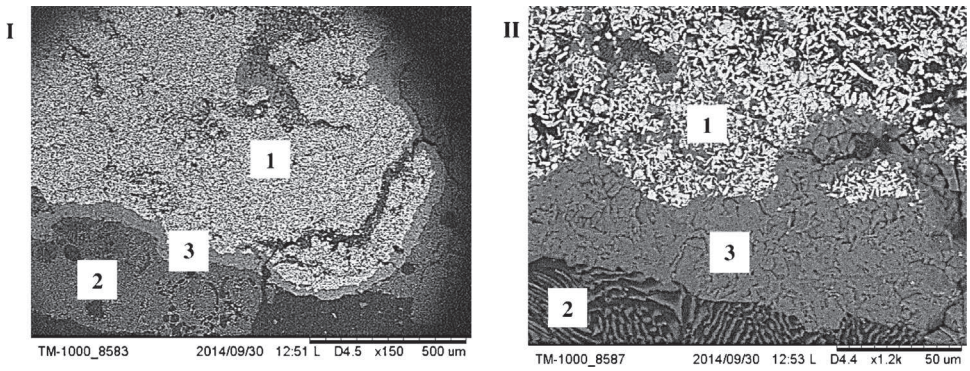

Fig. 2. (I and II) Micrographs of Nd_2O_3 pellet cross-section after electrolysis ($I = -0.4$ A and $t = 1320$ s) at 900 °C in LiF–CaF_2–Li_2O (2 mass % Li_2O).

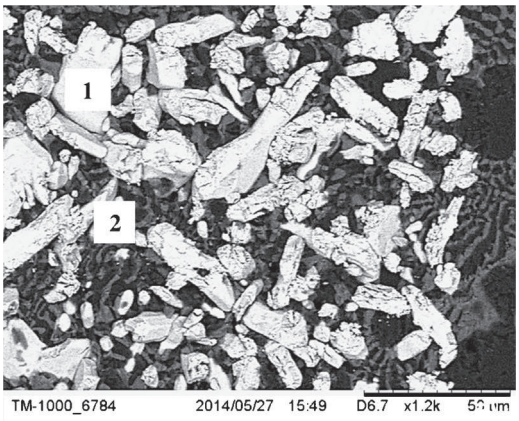

Fig. 3. Micrograph of Nd_2O_3 pellet cross-section after electrolysis ($I = -0.4$ A, 500% Q_{th}) at 1040 °C in LiF–CaF_2–Li_2O (2 mass %).

porosity. This phenomena was also confirmed by the X-ray diffractogram (Fig. 4) where Nd_2O_3, LiF and CaF_2 are present, but no NdOF was detected.

To investigate the temperature effect, a Nd_2O_3 pellet was exposed at 1 040 °C in the molten salt bath without polarisation, and SEM analysis showed similar structures to those presented in Fig. 3. Batsanov et al. [39] had already observed a similar behaviour of neodymium oxide powder (grain size 1–10 μm) under high pressure and temperature, where 100–1000 μm crystalline aggregates were created.

The influence of the applied cathodic current (from 0.15 A to 0.8 A) and neodymium oxide pellets fabrication (pressure applied for sinterizing the oxide powder from 2 to 4 t cm^{-2}) was also studied, but metallic neodymium was still not obtained.

To resume, Nd_2O_3 electrochemical reduction did not lead to metallic neodymium, whatever the operating parameters. Moreover, several limiting phenomena were highlighted:

1 Related to Nd_2O_3 physicochemical characteristics:

- low electrical conductivity ($\sigma_{650\ °C,0,2barO2} = 1{,}45 \times 10^{-6}\ \Omega^{-1}\ cm^{-1}$) [33];
- unfavourable Pilling-Bedworth coefficient ($V_{Nd}/V_{Nd2O3} = 0.89$). Pilling–Bedworth rule considerations [40], as illustrated by Li et al. [41] and Gibilaro et al. [42], indicate that during oxide reduction, if the molar volume of the formed metal *V*m is smaller than the molar volume of the oxide *V*o, the metal obtained is porous enough to allow the molten salt electrolyte accessing the underlying oxide. For neodymium, the metal to oxide molar volume ratio is $V_{Nd}/V\ Nd_2O_3 = 0.89$, meaning that volume constriction is not enough during Nd_2O_3 conversion into metal: the metallic neodymium formed would thus act as a diffusion barrier.

2 Related to solvent:

- neodymium oxide can only be reduced by Ca metal, limiting the selection to CaF_2-based solvents;
- in CaF_2-based solvent, at 900 °C, the precipitation of a dense insoluble CaO layer on the sample surface is observed, preventing Nd_2O_3 reduction.

2.4. Reduction of neodymium oxide in presence of copper oxide

To obtain metallic Nd, the addition of an electrical conducting oxide in the neodymium oxide pellet was tested. CuO was chosen for its good electrical conductivity ($\sigma_{127\ °C} = 10^{-1}\ \Omega^{-1}\ cm^{-1}$ [43]) and its favourable Pilling–Bedworth coefficient $V_{Cu}/V_{CuO} = 0.56$

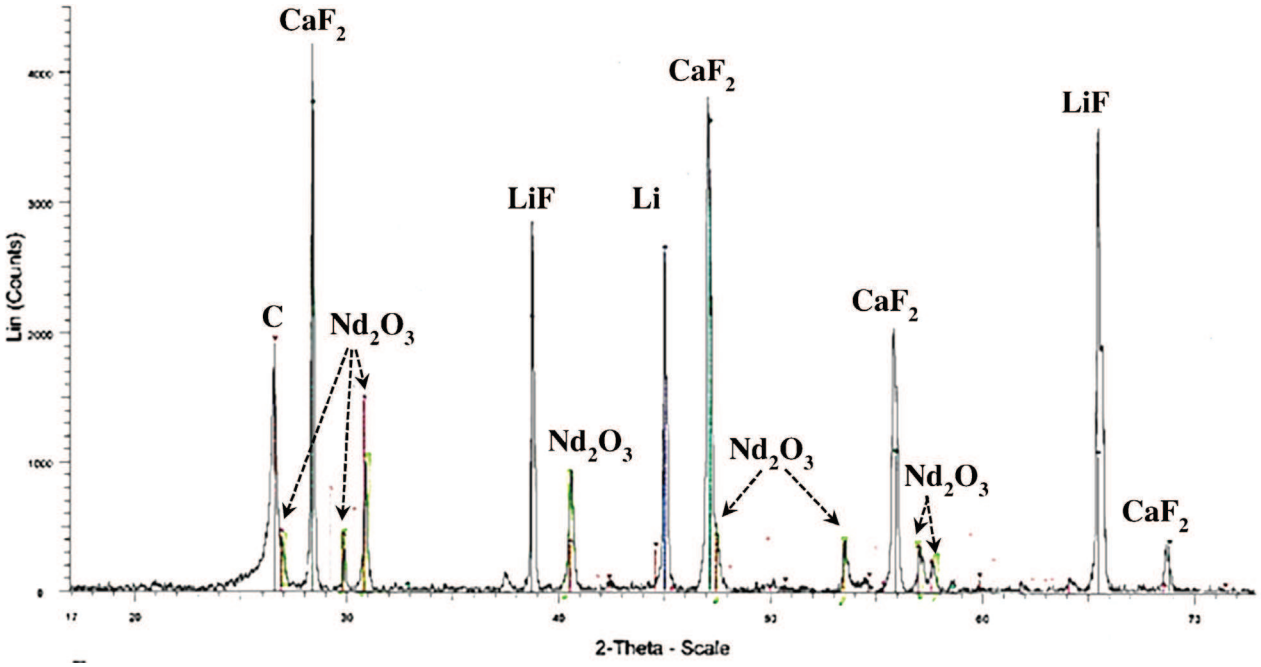

Fig. 4. X-ray diffractogram of Nd_2O_3 pellet after electrolysis ($I = -0.4$ A, 500% Q_{th}) at 1 040 °C in LiF–CaF_2–Li_2O (2 mass %).

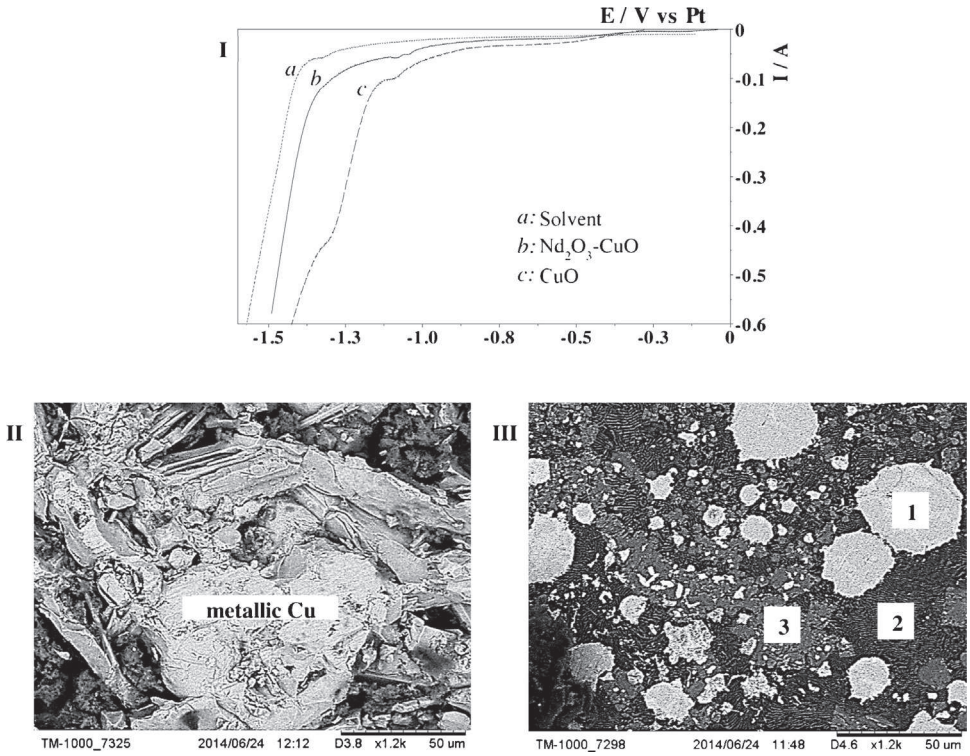

Fig. 5. **I** Linear sweep voltammograms in LiF–CaF_2–Li_2O (2 mass %) at 10 mV s^{-1} and 900 °C. Dotted line: solvent, continuous line: Nd_2O_3–CuO, interrupted line: CuO. **II, III** Micrographs of pellets cross-sections after electrolyses (I = −0.15 A, 500% Q_{th}) at 900 °C in LiF–CaF_2–Li_2O (2 mass %). **II.** CuO; **III.** Nd_2O_3–CuO: 65 atomic % Nd − 35 atomic % Cu.

[36], enhancing pellet porosity. CuO is therefore expected to undergo direct electrochemical reduction into metallic Cu, and to confirm it, CuO reduction in LiF–CaF_2–Li_2O (2 mass %) was first studied. The linear voltammogram obtained at 10 mV s^{-1} (voltammogram *c* in Fig. 5, I) displays a reduction signal at −1.3 V vs Pt, assigned to the direct electrochemical reduction of CuO into metallic Cu, following the equation:

$$CuO + 2e^- \rightarrow Cu + O^{2-} \quad (7)$$

Moreover, the electrolysis of a CuO pellet at −0.15 A and 900 °C confirmed this result: 100 μm to 1000 μm metallic Cu clusters (micrograph in Fig. 5, II) were obtained.

The current efficiency was also calculated, following the equation:

$$\eta = \frac{m_{experimental}}{m_{theoretical}}$$

where $m_{experimental}$ is the mass of the metallic deposit obtained by electrolysis (g) and $m_{theoretical}$ is the theoretical mass of metallic deposit expected to be obtained by electrolysis (g), calculated as following:

$$m_{theoretical} = {}^{I} * t/_{n} * F * M_{metal}$$

where I is the intensity of the imposed current (A), t is electrolysis duration (s), n is the number of exchanged electrons per mole of metallic oxide (n = 2 for CuO → Cu reduction), F is the Farady constant (96 480C mol^{-1}), and M_{metal} is the atomic mass of the metal (for Cu, M = 63,54 g mol^{-1}).

The calculated current efficiency for CuO reduction into metallic Cu was very close to 100%.

Nd_2O_3 reduction in presence of CuO was further investigated. Cu–Nd phase diagram [44] presents several liquid and solid alloys, and composition of Nd_2O_3–CuO pellets was chosen to be in the zone where liquid alloys are formed: 65 atomic % Nd and 35 atomic % Cu. The linear voltammogram of Nd_2O_3–CuO at 10 mV s^{-1} in LiF–CaF_2–Li_2O (2 mass %) (voltammogram *b* in Fig. 5, I) shows also a reduction signal starting from −1.4 V vs Pt, due to the direct electrochemical reduction of CuO. Additional cathodic signals, between −1.0 and −1.3 V vs Pt, were assigned to impurities present in the solvent (compared to voltammogram *a* in Fig. 5, I) and in the 99% purity CuO (comparison with voltammogram *c* in Fig. 5, I). After electrolysis at −0.15 A (500% Q_{th}) and 900 °C, the sample presented several zones (Fig. 5, III):

- Zone 1, composed of $NdCu_4$, $NdCu_5$ and $NdCu_6$ droplets (size < 50 μm);
- Zone 2, composed of recrystallized LiF and CaF_2;
- Zone 3, composed of NdOF and CaO, but no compact layer is observed on sample surface.

These results confirm Nd_2O_3 reduction is possible when CuO is simultaneously present, leading to formation of Cu–Nd alloys, and a multi-step reduction mechanism was proposed, as follows:

1st step: Chemical decomplexation of Nd_2O_3 into NdOF:

$$Nd_2O_3 + 2F^- \rightarrow 2NdOF + O^{2-} \quad (6)$$

2nd step: CuO direct reduction at the cathode, leading to metallic Cu, behaving as reactive cathode:

$$\text{Mo cathode: } CuO + 2e^- \rightarrow Cu + O^{2-} + \text{porosity} \quad (7)$$

3rd step: NdOF reduction on the surface of metallic Cu, leading to Cu-Nd alloys:

$$\text{Metallic Cu reactive cathode: } Cu + NdOF + 3e^- \rightarrow Cu\text{–}Nd + O^{2-} + F^- \quad (8)$$

The third step of this mechanism was confirmed by electrolyses of Nd_2O_3-Cu metallic powder mixture, which also led to the formation of Cu–Nd alloys. Nourry et al. presented also similar results, showing that Nd^{3+} reduction on copper cathode led to formation of Cu–Nd alloys [37,45,46].

Several authors proved the reduction of rare earth oxides in presence of metallic oxides to be suitable for obtaining rare earth alloys in molten chlorides. Moreover, they also proposed reduction mechanisms where the metallic oxide (Co_3O_4, NiO, Co_3O_4, Fe_2O_3) was first reduced on the cathode, followed by the reduction of rare earth oxide and formation of alloys [27–32].

The current efficiencies for Nd_2O_3 reduction in presence of CuO or metallic Cu powder could not be estimated, due to the lack of homogeneity of the sample and the small size of Cu–Nd alloys droplets (<50 μm diameter, Fig. 5, III), which could not be fully recovered to be weighted.

Nevertheless, when Nd_2O_3–CuO electrolyses were performed at higher temperature (1040 °C), coalescing of Cu–Nd droplets occurred (size∼500 μm to 2 mm), facilitating their recovery at the end of electrolysis. In this case, the global current efficiency could be estimated using the equation (8) and its value was ∼70%. The remaining 30% current fraction could be related to solvent reduction (Ca^+ and Li^+) and uncomplete recovery and separation of Cu–Nd alloys from the salt.

The reduction of neodymium oxide in presence of copper oxide presents several advantages:

- CuO direct reduction led to creation of porosity in the pellet, enabling the penetration of molten salt in the bulk of the sample and thus enhancing the interaction between the solvent, the metallic Cu obtained by reduction and the neodymium oxide;
- Under polarization, the metallic copper obtained by CuO direct reduction behaves as reactive cathodic material, leading to formation of Cu–Nd alloys.

To recover high purity metallic Nd, Cu and Nd separation can be easily accomplished by the electrorefining process, due to the large differences of their electrochemical potentials: in LiF–CaF_2 at 840 °C, $E_{Cu^{2+}/Cu} = 2.83$ V/Li^+/Li and $E_{Nd^{3+}/Nd} = 0.35$ V/Li^+/Li [37]. Thus, Nd from Cu-Nd alloys can be selectively oxidized into Nd(III), which will be further deposited as high purity metallic Nd on the cathode. Meanwhile, pure metallic Cu remaining at the anode can be recycled and reused for Nd_2O_3 reduction.

3. Conclusions

In molten fluoride media, the reduction of Nd_2O_3 was shown to be indirect, similar to the OS process. Nevertheless, reduction of neodymium oxide into metallic neodymium did not occur when using an inert cathodic material (Mo), regardless of the operating parameters (temperature, current, fabrication of the oxide pellet). The limiting factors were related to the:

1. Physical characteristics of Nd_2O_3: low conductivity and unfavourable Pilling-Bedworth coefficient.
2. Solvent: Indirect reduction of Nd_2O_3 in molten salts is thermodynamically achievable ($\Delta_r G° < 0$) for Ca-based solvents only, when metallic Ca is obtained. However, a dense insoluble CaO layer was formed overall the sample surface, acting as diffusion barrier for O^{2-}, preventing the reduction of the oxide pellet.

Moreover, Nd_2O_3 behavior was influenced by temperature: at 900 °C, the oxide was decomplexed into insoluble chemically stable NdOF, while at 1040 °C it led to formation of crystalline aggregates. Thus, electrowinning of metallic neodymium from neodymium oxide cannot be performed in molten fluoride media in absence of NdF_3.

Addition of a conductive metallic oxide to the neodymium oxide was further investigated. When Nd_2O_3–CuO and Nd_2O_3–Cu pellets were electrolyzed, metallic neodymium was recovered as alloyed Cu–Nd droplets, and at higher temperature (T > 1 040 °C) a better coalescence was observed. The following reduction mechanism was proposed:

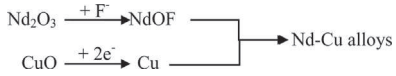

The Cu, initially present in mixture with Nd_2O_3 or produced by CuO direct electroreduction, acts as a depolarizing reactive cathode for Nd^{3+} (NdOF) reduction, leading to Cu–Nd alloys. This strategy is the only one viable for obtaining metallic Nd from neodymium oxide in molten fluorides without NdF_3. Furthermore, high purity metallic Nd can be recovered by a simple electrorefining process, while the metallic Cu can be recycled and reused for Nd_2O_3 reduction.

4. Experimental

The cell design consisted in a vitreous carbon crucible placed in a cylindrical vessel made of refractory steel. The inner part of the cell wall was protected against fluoride vapours by a graphite liner. Experiments were performed under inert argon atmosphere. The molten salt (200 g) was composed of LiF-CaF_2 eutectic, dehydrated by heating under vacuum from room temperature up to melting point (767 °C). Li_2O powder (Cerac 99.5%) was used to provide O^{2-} ions in the bath, to ensure the anodic reaction ($2O^{2-} \rightarrow O_2 + 4e^-$). Nd_2O_3 (Aldrich 99.9%), CuO (Merck 99%) and Cu metallic powder (Goodfellow 99.8%) were used in the form of pellets sintered by applying a pressure of 3.2 t cm^{-2} to several milligrams (from 100 to 300 mg) of powder, at 25 °C. The pellets, attached with a molybdenum grid connected to the current lead by a molybdenum wire, were used as working electrodes. The auxiliary electrode was a gold wire or plate, with a large surface area (S = 3 cm^2), and all potentials were referred to a platinum wire (0.5 mm diameter), acting as a quasi-reference electrode Pt/PtO_x/O^{2-}.

The electrochemical experiments were performed with an Autolab PGSTAT 30 potentiostat-galvanostat. After resin embedding and polishing, the cathode bulk was examined with a scanning electron microscope SEM (LEO 435 VP) equipped with and EDS probe (Oxford INCA 200). XRD characterisations were performed with an Equinox 1000 diffractometer. Quantitative analysis were performed with a Cameca SXFive electron probe microanalyser. Nevertheless, neither SEM-EDS nor electron-probe microanalysis do not provide data on Li. Meanwhile, SEM-EDS do not provide data analysis on light elements such as fluoride and oxygen.

References

[1] K. Binnemans, P.T. Jones, B. Blanpain, T. Van Gerven, Y. Yang, A. Walton, M. Buchert, J. Cleaner Prod. 51 (2013) 1–22.
[2] E. Morrice, E.S. Shed, T.A. Henrie, U.S. Bur. Mines Rep. Invest. 7146 (1968).
[3] E. Morrice, M.M. Wong, Miner. Sci. Eng. 11 (1979) 125–136.
[4] Y. Qiqin, L. Guanqun, F. Zhongan, S. Lichang, Rare Met. 8 (1989) 9.
[5] M.F. Chambers, J.E. Murphy, U.S. Bur. Mines Rep. Invest. 9391 (1991).
[6] A. Kaneko, Y. Yamamoto, C. Okada, J. Alloys Compd. 193 (1993) 44–46.
[7] C. Shiguan, Y. Xiaoyong, Yu. Zhongwing, Lu. Qingtao, Rare Met. 13 (1994) 46.
[8] J.E. Murphy, D.K. Dysinger, M.F. Chambers, Light Met. (1995) 1313–1320.
[9] D.W. Dees, J.P. Ackerman, University of Chicago, US Patent 0045835 A1, (2004).
[10] Y.H. Kang, S.C. Hwang, H.S. Lee, E.H. Kim, J. Met. Process. Technol. 209 (2009) 5008–5013.
[11] R. Fujita, H. Nakamura, K. Mizuguchi, S. Kanamura, T. Omori, K. Utsunomyia, S. Nomura, Kabushiki Kaisha Toshiba, US Patent 0314260 A1, (2010).
[12] B.H. Park, I.C. Choi, J.-M. Hur, J. Chem. Eng. Japan 45 (2012) 888–892.
[13] E.-Y. Choi, J.W. Lee, J.J. Park, J.-M. Hur, J.-K. Kim, Chem. Eng. J. 514 (2012) 207–208.
[14] S. Seetharaman (Ed.), Treatise on Process Metallurgy, vol. 3, Elsevier, 2014, pp. 995–1069.
[15] E. Stefanidaki, C. Hasiotis, C. Kontoyannis, Electrochim. Acta 46 (2001) 2665–2670.

[16] E. Stefanidaki, G.M. Photiadis, C. Kontoyannis, A. Vik, T. Østvold, J. Chem. Soc. (2002) 2302–2307.
[17] R. Thudum, A. Srivastava, S. Nandi, A. Nagaraj, R. Shekhar, Min. Process. Extr. Metall. (Trans. Inst. Min. Metall. C) 119 (2010) 88–92.
[18] D.K. Dysinger, J.E. Murphy, US Bur. Mines Rep. Invest. 9504 (1994).
[19] E. Morrice, E. Shedd, T. Henrie, US Bur. Mines Rep. Invest. 7146 (1968).
[20] Y. Bertaud, Aluminium Pechiney, European Patent EP0289434 (A1), 1988.
[21] D. Chen, Solution of Neodymium and formation of slime during the neodymium electrolysis, J. Rare Met. 32 (2008) 482–483 Translated from Chinese by J. Wang, in Chinese.
[22] W. Li, Utilization rate of neodymium oxide in producing metallic neodymium, Non-ferrous Smelting 4 (50) (2001) 35–36 Translated from Chinese by J. Wang.
[23] E. Morrice, R.G. Reddy, Solubility of rare earth oxides in fluoride melts, Symposium on High Temperature and Materials Chemistry, Berkeley, California, 1989.
[24] X. Guo, J. Sietsma, Y. Yang, 1st European Rare Earth Resources Conference 2014, Milos Island, Greece, 4–7 September, 2014, pp. 149.
[25] G.Z. Chen, D.J. Fray, T.W. Farthing, Nature 407 (2000) 361–364.
[26] K. Ono, R.O. Suzuki, J. Min. Metals Mat. Soc. 54 (2002) 59–61.
[27] A.M. Abdelkader, D.J. Hyslop, A. Cox, D.J. Fray, J. Mater. Chem. 20 (2010) 6039–6049.
[28] B.J. Zhao, L. Wang, L. Dai, G.G. Cui, H.Z. Zhou, J. Alloys Compd. 468 (2009) 379–385.
[29] L. Dai, S. Wang, Y.-H. Li, L. Wang, Trans. Nonferrous Met. Soc. China 22 (2012) 2007–2013.
[30] Y. Zhang, H. Yin, S. Zhang, D. Tang, Z. Yuan, T. Yan, W. Zheng, J. Rare Earths 30 (2012) 923–927.
[31] G. Qiu, D. Wang, M. Ma, X. Jin, G.Z. Chen, J. Electroanal. Chem. 589 (2006) 139–147.
[32] G. Qiu, D. Wang, X. Jin, G.Z. Chen, Electrochim. Acta 51 (2006) 5785–5793.
[33] K.A. Gschneider Jr., L. Eyring, Handbook on the Physics and Chemistry of Rare Earths Ch. 27, North-Holland Publishing Comp., 1979, pp. 386.
[34] M. Gibilaro, S. Bolmont, L. Massot, P. Chamelot, J. Electroanal. Chem. 726 (2014) 84–90.
[35] M. Gibilaro, L. Cassayre, O. Lemoine, L. Massot, P. Chamelot, J. Nucl. Mater. 414 (2011) 169–173.
[36] L. Massot, L. Cassayre, P. Chamelot, P. Taxil, J. Electroanal. Chem. 606 (2007) 17–23.
[37] C. Nourry, Thèse de doctorat de l'Université Paul Sabatier, Toulouse (2007) 51.
[38] D.-G. Kim, M.-A. Van Ende, C. Liebske, C. van Hoek, S. van der Laan, P. Hudon, I.-H. Jung, 9th International Conference on Molten Slags, Fluxes and Salts, Beijing, China, 27–30 May, 2012, pp. 110.
[39] S.S. Batsanov, A.A. Deribas, Fizika Goreniya I Vzryva 1 (1965) 103–108 English version: Combustion, Explosion and Shock Waves 1 (1965) 77–80 (10.1007/2FB00757157)..
[40] N.B. Pilling, R.E. Bedworth, J. Inst. Met. 29 (1923) 529–591.
[41] W. Li, X. Jin, F. Huang, Angew. Chem. Int. Ed. 49 (2010) 3203–3206.
[42] M. Gibilaro, J. Pivato, L. Cassayre, L. Massot, P. Chamelot, Electrochim. Acta 56 (2011) 5410–5415.
[43] A.A. Samokhvalov, N.A. Viglin, B.A. Gizhevskĭi, N.N. Loshkareva, V.V. Osipov, N. I. Solin, Y.P. Sukhorukov, Zh. Eksp. Teor. Fiz. 103 (1993) 951–961 English version: J. Exp. Theor. Phys. 76 (1993) 462–468 (http://www.jetp.ac.ru/cgi-bin/dn/e_076_03_0463. pdf)..
[44] Binary Alloy Phase Diagrams, S.E., ASM International, 1996.
[45] C. Nourry, L. Massot, P. Chamelot, P. Taxil, J. Appl. Electrochem. 39 (2009) 927–933.
[46] C. Nourry, L. Massot, P. Chamelot, P. Taxil, J. Appl. Electrochem. 39 (2009) 2359–2367.